Bistable Behavior in a Model of the *lac* Operon in *Escherichia coli* with Variable Growth Rate

M. Santillán
Unidad Monterrey, Centro de Investigación y Estudios Avanzados del IPN, Monterrey, México, and Centre for Nonlinear Dynamics in Physiology and Medicine, McGill University, Montreal, Canada

ABSTRACT This work is a continuation from another study previously published in this journal. Both the former and the present works are dedicated to investigating the bistable behavior of the *lac* operon in *Escherichia coli* from a mathematical modeling point of view. In the previous article, we developed a detailed mathematical model that accounts for all of the known regulatory mechanisms in this system, and studied the effect of inducing the operon with lactose instead of an artificial inducer. In this article, the model is improved to account, in a more detailed way, for the interaction of the repressor molecules with the three *lac* operators. A recently discovered cooperative interaction between the CAP molecule (an activator of the lactose operon) and Operator 3 (which influences DNA folding) is also included in this new version of the model. The growth rate dependence on the rate of energy entering the bacteria (in the form of transported glucose molecules and of metabolized lactose molecules) is also considered. A large number of numerical experiments is carried out with this improved model. The results are discussed in regard to the bistable behavior of the lactose operon. Special attention is paid to the effect that a variable growth rate has on the system dynamics.

INTRODUCTION

In 1960, Jacob et al. (1) introduced the operon concept as a consequence of their studies on the control of lactose metabolism in *Escherichia coli*. Concomitantly, they discovered an ubiquitous mechanism for gene regulation: repression. In the *lac* operon, a repressor molecule can bind a specific site along the DNA molecule (see Figs. 1 and 2) to halt transcription of the operon structural genes. One of the *lac* operon genes encodes for a membrane permease protein, which transports lactose into the cell. Intracellular lactose is degraded into glucose and galactose by β-galactosidase, an enzyme encoded for by another gene in the *lac* operon. Furthermore, allolactose (a by-product of lactose metabolism) binds and inactivates the repressor molecules, thus halting repression of the expression of the structural genes. Thus, the lactose operon regulatory pathway involves a positive feedback loop, which can give rise to bistability (2).

The capacity of a system to switch in an all-or-none manner between alternative steady states, and the presence of hysteresis, are the hallmarks of bistability. Bistability has been invoked as a possible explanation for catastrophic events in ecology (3), mitogen-activated protein kinase cascades in animal cells (4–6), cell cycle regulatory circuits in *Xenopus* and *Saccharomyces cerevisiae* (7,8), the generation of switchlike biochemical responses (4,5,9), and the establishment of cell cycle oscillations and mutually exclusive cell cycle phases (8,10). More recently, Dubnau and Losick (11) discussed the possible evolutionary advantages of the heterogeneity in bacteria populations emerging from bistability.

The bistable behavior of the *lac* operon has been the subject of a number of investigations. Signs of bistability were first noted by Monod and co-workers more than fifty years ago, although it was not fully recognized at the time. The first detailed studies were performed by Novick and Weiner (12) and Cohn and Horibata (13). Further experimental research was carried out by Maloney and Rotman (14) and Chung and Stephanopoulos (15).

In a recent article, Ozbudak et al. (16) reported a set of ingenious experiments that allowed them to quantify the *lac*-operon expression level in single bacteria. Their results not only confirmed the existence of bistability in the *lac* operon when induced with the nonmetabolizable inducer thio-methylgalactoside (TMG), but also raised important questions. Namely, when Ozbudak et al. repeated their experiments using lactose as inducer, they found no evidence for bistability. We investigated this issue from a mathematical modeling viewpoint in a previous article (17). There, we developed a mathematical model for the *lac* operon regulatory pathway, and used it to investigate the effect that inducing the operon with lactose has on the system bistable behavior.

In this article, we extend this investigation by taking into account some further, recently discovered, details of the *lac* operon regulatory mechanisms. Namely: the repressor molecule—which is a tetramer made up of two functional dimers—can still bind a single operator if one of its dimers is free from lactose (18), and the activator CAP facilitates the formation of a DNA loop between Operators 1 and 3 (19). Additionally, we consider in this model the fact that the bacterial growth-rate varies in accordance to the glucose uptake and the lactose metabolism rates, and study how this affects the system dynamic behavior.

Submitted July 23, 2007, and accepted for publication November 16, 2007.

Address reprint requests to M. Santillán, E-mail: moises.santillan@mac.com.

Editor: Arthur Sherman.

0006-3495/08/03/2065/17 $2.00

doi: 10.1529/biophysj.107.118026

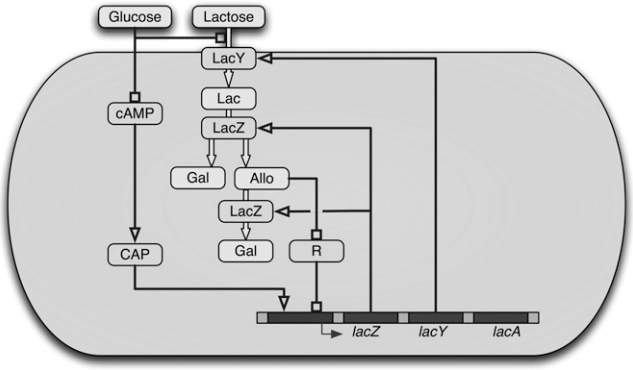

FIGURE 1 Schematic representation of the *lac* operon regulatory pathway. Figure was taken from Santillán et al. (17).

THEORY

Mathematical model

In Appendix A, a mathematical model for the lactose operon is developed. This model is an improvement and generalization of the one introduced in Santillán et al. (17). In this new model, we take into account more details of the interaction between *lac* repressor and inducer (lactose or TMG) molecules. Specifically, instead of assuming—as in Santillán et al. (17)—that only free repressors can bind an operator, we take into account the fact that a repressor bound with one or two inducers in the same side can be active (see Fig. 2). There is new evidence that, when bound to its corresponding site, a CAP molecule not only increases the probability that a polymerase binds the promoter, but also facilitates the formation of a DNA loop in such a way that a single repressor binds Operators 1 and 3 (19). The present version of the model, unlike the previous one, takes into consideration this new source of cooperativity by assuming that the binding of a CAP molecule and the formation of the Operator 1:Repressor:Operator 3 loop only happen simultaneously. Finally, the model in Santillán et al. (17), as many others, assumes a constant growth rate (μ). This situation corresponds to an experimental setup in which the growing medium is rich in a substance like succinate, which, acting as a reliable carbon source, ensures a high growth rate for the bacterial culture, and affects neither the glucose nor the lactose uptake and metabolism. In the present model, we consider a variable growth rate that depends on the glucose uptake rate as well as on the rate of lactose metabolism. This refinement to the model allows us to simulate a bacterial culture growing in a medium containing a mixture of glucose and lactose, and no other carbon source.

A glossary of all the model variables and parameters is given in Table 1. A general description of the model equations, presented in Table 2, is given below. To follow this description, the reader may find it useful to refer to Figs. 1 and 2, which present schematic representations of the *lac* operon regulatory pathway and of the regulatory elements located in operon DNA.

The present model consists of three ordinary differential equations that account for the dynamics of the *lacZ* messenger RNA (Eq. 1), LacZ polypeptide (Eq. 2), and intracellular lactose (Eq. 3) concentrations. Messenger RNA (mRNA) is produced via transcription of the *lac* operon genes, and its concentration decreases because of active degradation and dilution due to cell growth. The dependence of the growth rate μ on the glucose uptake rate J_G (defined in Eq. 17), and on the lactose metabolism rate J_L (defined in Eq. 18), is given in Eq. 7.

$\mathcal{P}_R(A)$ (defined in Eq. 11) accounts for regulation of transcription initiation by active repressors. This function gives the probability that the *lac* promoter is not repressed by an active repressor bound to Operator O_1. It accounts for the interactions of the repressor and allolactose molecules, of the repressor molecules and the three different *lac* operators (including DNA looping), of the CAP activator and the mRNA polymerase, and of CAP and the DNA loop involving Operators 1 and 3.

Repressor molecules are tetramers formed by the union of two active dimers. Every one of the four repressor subunits can be bound by an allolactose molecule. Free repressors, repressors bound by one allolactose, and repressors bound by two allolactoses in the same dimer can bind a single operator

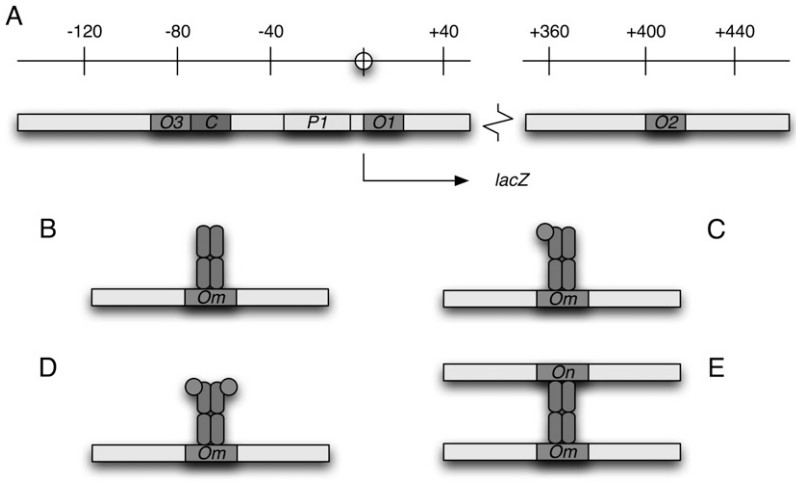

FIGURE 2 (*A*) Schematic representation of the regulatory elements located in *lac* operon DNA. P_1 denotes the promoter, O_1, O_2, and O_3 correspond the three operators (repressor binding sites), and *C* is the binding site for the cAMP-cAMP receptor protein complex. The different ways in which a repressor molecule can interact with the operator sites are represented in *B–E*. Namely, a free repressor molecule (*B*), one with a single subunit bound by allolactose (*C*), or one with the two subunits in the same side bound by allolactose (*D*) can bind a single operator. Moreover, a free repressor molecule can bind two different operators simultaneously.

TABLE 1 Glossary of variables and parameters in the model equations

$[M]$	Concentration of *lac*Z mRNA.
$[E]$	Concentration of LacZ polypeptides.
$[L]$	Intracellular lactose concentration.
$[D]$	Concentration of *lac* operon copies per bacterium.
$[A]$	Intracellular allolactose concentration.
$[Q]$	*lac* permease concentration.
$[B]$	β-galactosidase concentration.
ϕ_M	Maximum lactose-to-allolactose conversion rate per β-galactosidase.
μ	Bacterial growth rate.
γ_M	*lac*Z mRNA degradation rate.
γ_E	LacZ polypeptide degradation rate.
k_M	Maximal transcription initiation rate of the *lac* promoter.
k_E	Translation initiation rate of the *lac*Z transcript.
k_L	Maximal lactose uptake rate per permease.
p_p	Probability that a polymerase is bound to the *lac* promoter.
p_c	Probability that a CAP complex is bound to its binding site.
p_{pc}	Probability that both a polymerase and a CAP complex are bound to their sites.
k_{pc}	Parameter that accounts for the cooperativity between the promoter and the CAP sites.
K_G and n_h	Parameters that determine the dependence of p_c on Ge.
$\mathcal{P}_R$	Probability that a polymerase is bound to the promoter, and ready to start transcription.
ξ_i	Parameter that determines the affinity of an active repressor for Operator O_i.
ξ_{ij}	Parameter that determines the stability of the O_i-repressor-O_j complex.
ρ_1	Probability that a repressor molecule is able to bind a single operator.
ρ_2	Probability that a repressor molecule is able to bind two operators simultaneously.
K_A	Dissociation constant for the repressor-allolactose complex formation reaction.
β_L	Permease activity as a function of the external lactose concentration.
κ_L	Half-saturation constant for the lactose uptake rate.
β_L	Permease activity as a function of the external glucose concentration.
ϕ_G and κ_G	Parameters that determine the dependence of β_L on Ge.
$\mathcal{M}$	Lactose-to-allolactose metabolism rate per β-galactosidase.
J_G	Glucose uptake rate.
J_G^{max}	Maximum glucose uptake rate.
Φ_G	Half-saturation constant for the glucose uptake rate.
J_L	Production rate of glucoselike molecules via lactose metabolism.

(18). The fraction of repressors able to do so is $\rho_1(A)$ (compare to Eq. 12). Conversely, only free repressors, whose fraction is given by $\rho_2(A)$ (see Eq. 13), can bind two different operators simultaneously.

The function $p_{pc}(Ge)$ (Eq. 8) denotes the modulation of transcription initiation by the cooperative interaction between a CAP activator and a polymerase, each bound to its respective site. Production of cyclic AMP (cAMP) is inhibited by extracellular glucose. cAMP further binds the so-called cAMP receptor protein to form the CAP complex. Finally, CAP binds a specific site near the *lac* promoter and enhances transcription initiation. The probability of finding a CAP molecule bound to its corresponding site is given by p_c (Eq. 10).

The probability that a CAP activator is bound to its corresponding site is given by the function $p_{cp}(Ge)$ (Eq. 9). Its presence in the definition of $\mathcal{P}_R(A)$ (Eq. 11) accounts for the fact that it affects the formation of the DNA loop in which a single repressor binds Operators 1 and 3.

Let B and Q, respectively, denote the β-galactosidase and permease concentrations. The translation initiation rate of *lacZ* transcripts is k_E, while γ_E is the degradation rate of *lacZ* polypeptides. Given that the corresponding parameters for *lacY* transcripts and polypeptides attain similar values, that β-galactosidase is a homo-tetramer made up of four identical *lacZ* polypeptides, and that permease is a *lacY* monomer, it follows that $Q = E$ and $B = E/4$ (Eqs. 5 and 6).

Lactose is transported into the bacterium by a catalytic process in which permease proteins play a central role. Thus, the lactose influx rate is assumed to be $k_L\beta_L(Le)Q$, with the function $\beta_L(Le)$ given by Eq. 14. Extracellular glucose inhibits lactose uptake, a mechanism known as inducer exclusion, and this is accounted for by $\beta_G(Ge)$ (Eq. 15). Once inside the cell, lactose is metabolized by β-galactosidase. Approximately half of the lactose molecules are transformed into allolactose, while the rest enter the catalytic pathway that produces glucose and galactose. In our model, $\phi_M\mathcal{M}(L)$, with $\mathcal{M}$ defined in Eq. 16, denotes the lactose-to-allolactose metabolism rate, which equals the lactose-to-galactose metabolism rate. Allolactose is further metabolized into galactose by β-galactosidase. From the assumptions that the corresponding metabolism parameters are similar to those of lactose, and that the allolactose production rate is much higher than its degradation plus dilution rate, it follows that $A \approx L$ (Eq. 4).

Parameter values

Except for K_A, all the parameters in the model are estimated from experimental results in Appendix B and tabulated in Table 3. Parameter K_A remains as a free parameter that will be estimated by fitting the model results to those obtained experimentally by Ozbudak et al. (16).

METHODS

Calculation of the bifurcation diagrams

If the growth rate (μ), which is variable as detailed in the equations of Table 2, is held at a constant value, it can be shown after a little algebra that the L steady-state values are those that satisfy the following equation:

$$[D]\frac{k_M k_E k_L}{\mu(\mu+\gamma_E)(\mu+\gamma_M)}\,p_{pc}([Ge])\mathcal{P}_R([L]) \times\left(\beta_L([Le])\beta_G[Ge]-\frac{\phi_M}{2k_L}\mathcal{M}([L])\right)=[L]. \quad (19)$$

Depending on $[Ge]$ and $[Le]$, Eq. 19 has up to three roots, which correspond to the uninduced and induced stable steady states, separated by an unstable saddle node. The uninduced and induced states may appear (together with the saddle node) and disappear (by colliding with the saddle node) via a saddle node bifurcation as $[Le]$ varies. The mathematical conditions for the

TABLE 2 A mathematical model for the *lac* operon in *E. coli*

$$[\dot{M}] = k_M[D]p_{pc}([Ge])\mathcal{P}_R([A]) - (\gamma_M + \mu)M. \quad (1)$$

$$[\dot{E}] = k_E[M] - (\gamma_E + \mu)[E]. \quad (2)$$

$$[\dot{L}] = k_L\beta_L([Le])\beta_G([Ge])[Q] - 2\phi_M\mathcal{M}([L])[B] - \mu[L]. \quad (3)$$

$$[A] = [L]. \quad (4)$$

$$[Q] = [E]. \quad (5)$$

$$[B] = [E]/4. \quad (6)$$

$$\mu = \varepsilon(J_G([Ge]) + J_L([L])). \quad (7)$$

$$p_{pc}([Ge]) = \frac{p_p\left(1 + p_c([Ge])\left(k_{pc} - 1\right)\right)}{1 + p_p p_c([Ge])\left(k_{pc} - 1\right)}. \quad (8)$$

$$p_{cp}([Ge]) = \frac{p_c\left(1 + p_p([Ge])\left(k_{pc} - 1\right)\right)}{1 + p_p p_c([Ge])\left(k_{pc} - 1\right)}. \quad (9)$$

$$p_c([Ge]) = \frac{K_G^{n_h}}{K_G^{n_h} + [Ge]^{n_h}}. \quad (10)$$

$$\mathcal{P}_R([A]) = \frac{(1 + \xi_2\rho_1([A]))(1 + \xi_3\rho_1([A])) + \xi_{23}\rho_2([A])}{\prod_{i=1,2,3}(1 + \xi_i\rho_1([A])) + \sum_{\substack{\sigma \in P(1,2,3) \\ \sigma_2 < \sigma_3}} \left(1 + (p_{cp} - 1)\delta_{2\sigma_1}\right)\left(1 + \xi_{\sigma_1}\rho_1([A])\right)\xi_{\sigma_2\sigma_3}\rho_2([A])}. \quad (11)$$

$$\rho_1([A]) = \left(\frac{K_A}{K_A + [A]}\right)^2. \quad (12)$$

$$\rho_2([A]) = \left(\frac{K_A}{K_A + [A]}\right)^4. \quad (13)$$

$$\beta_L([Le]) = \frac{[Le]}{\kappa_L + [Le]}. \quad (14)$$

$$\beta_G([Ge]) = 1 - \phi_G\frac{[Ge]}{\kappa_G + [Ge]}. \quad (15)$$

$$\mathcal{M}([L]) = \frac{[L]}{\kappa_M + [L]}. \quad (16)$$

$$J_G([Ge]) = J_G^{max}\frac{[Ge]}{[Ge] + \Phi_G}. \quad (17)$$

$$J_L([L]) = 4\phi_M\mathcal{M}([L])[B]. \quad (18)$$

In Eq. 11, $P(1, 2, 3)$ stands for the set of all the permutations of $\{1, 2, 3\}$, and δ_{ij} is the Krönecker delta.

occurrence of these bifurcations are that Eq. 19 is satisfied, and that the derivatives, with respect to L, of both sides of Eq. 19 are also equal (see (20)). The values of $[Le]$ and $[L]$ such that these two conditions are satisfied, given the value of $[Ge]$, were numerically determined with the aid of Octave's algorithm fsolve. Finally, by repeating this process for several Ge values, the bifurcation diagram in the Le versus Ge parameter space can be drawn.

Given the model complexity, it was not possible to derive a simple equation whose solutions give the steady-state values when a variable growth rate is considered. Therefore, we implemented the following algorithm to find the bifurcation points:

1. For a given value of Ge, the model differential equations are numerically integrated (using the algorithm lsode of Octave) with $L_e = 0$ μM and the initial conditions $M = 0$ mpb, $E = 0$ mpb, and $L = 0$ mpb, for a time period of 2000 min to ensure that the system reaches the steady state.
2. The value of Le is increased and the model equations are solved again, using the last point of the previous numerical solution as the initial condition.
3. The last step is repeated iteratively until the value of Le is so high that the system shifts from the uninduced to the induced state. This value of Le corresponds to the upper border of the bistable region in the bifurcation diagram.

TABLE 3 Values of the parameters in the *lac* operon model equations presented in Table 2, as estimated in Appendix B

$[D] \approx 2$ mpb	$k_M \approx 0.18\ \text{min}^{-1}$
$\varepsilon \approx 5.2 \times 10^{-10}\ \text{mpb}^{-1}$	$\gamma_M \approx 0.46\ \text{min}^{-1}$
$p_p \approx 0.127$	$k_{pc} \approx 30$
$K_G \approx 2.6\ \mu\text{M}$	$n_h \approx 1.3$
$\xi_1 \approx 17$	$\xi_2 \approx 0.85$
$\xi_3 \approx 0.17$	$\xi_{12} \approx 1261.7$
$\xi_{13} \approx 430.6$	$\xi_{23} \approx 0$
$K_A \approx ?$ mpb	$k_E \approx 18.8\ \text{min}^{-1}$
$\gamma_E \approx 0.01\ \text{min}^{-1}$	$k_L \approx 6.0 \times 10^4\ \text{min}^{-1}$
$\phi_M \approx \in [0, 3.8 \times 10^4]\ \text{min}^{-1}$	$\kappa_L \approx 680\ \mu\text{M}$
$\phi_G \approx 0.35$	$\kappa_G \approx 1.0\ \mu\text{M}$
$\kappa_M \approx 7.0 \times 10^5$ mpb	$J_G^{max} \approx 4.4 \times 10^7\ \text{mpb min}^{-1}$
$\Phi_G \approx 22\ \mu\text{M}$	

Parameter K_A is the only parameter we were unable to estimate. The unit mpb stands for molecules per average bacterium.

4. Step 2 is repeated iteratively once more, but now decreasing the *Le* value, until the system switches back from the induced to the uninduced state. This value of *Le* corresponds to the lower border of the bistable region in the bifurcation diagram.
5. Finally, Steps 1–4 are repeated for several values of *Ge*.

Stochastic simulations

We carried out stochastic simulations with the model described in this section using Gillespie's Tau-Leap algorithm (21,22), which we implemented in Python.

Calculation of the transition rate constants between the induced and the uninduced states

Following Warren and ten Wolde (23,24), the rates of transition between the induced and uninduced states—when the *Ge* and *Le* values are such that bistability exists—are calculated as follows. First, we constructed new time series, S, from the time series of lactose (or TMG) values, L, resulting from the stochastic simulations. By definition, $S(t) = 1$, whenever $L(t) > L_1^*$, and $S(t) = 0$ otherwise, where L_1^* is the value of L at the unstable saddle node located between the uninduced and induced states. Then, the times the system spends in the uninduced and induced states are calculated from the time series S, as well as the histograms of residence times in both states. In all cases, these histograms can be fitted by exponential distributions of the form $H(t) = A \exp(-kt)$, where k is the corresponding transition rate constant. In what follows, the transition rate constants from the uninduced (induced) to the induced (uninduced) state shall be denoted as k_+ (k_-).

RESULTS

Comparison with experimental results

Ozbudak et al. (16) carried out experiments in which *E. coli* cultures were grown in the M9 minimal medium, with succinate as the main carbon source, supplemented with varying amounts of glucose and TMG. They engineered a DNA segment in which the *gfp* gene was under the control of the wild-type *lac* promoter, and inserted this segment into the chromosome of the cultured *E. coli* bacteria, at the λ-insertion site. In these mutant bacteria, Ozbudak et al. estimated the *lac* operon expression level in each bacterium by simply measuring the intensity of green fluorescence.

Ozbudak et al. observed that the histograms of fluorescence intensities were unimodal, and that the mean value corresponded to low induction levels of the *lac* operon, when the bacterial growth medium had low TMG levels. After the TMG concentration surpassed a given threshold, the histograms became bimodal, which can be viewed as evidence for bistability: the original (new) mode corresponds to the uninduced (induced) steady state. With further increments of the TMG concentration, the mode corresponding to the uninduced state disappeared, and the histogram became unimodal again. When the experiment was repeated by decreasing the concentrations of TMG, the opposite behavior was observed. Ozbudak et al. measured the range of TMG concentrations for which bistability was obtained, for several concentrations of external glucose. When they repeated the same experiments with the natural inducer (lactose), they were unable to find analogous evidence for bistability, even when lactose was given at saturation levels. In these last experiments, they employed glucose concentrations in the same range as in the experiments with TMG.

Following Santillán et al. (17), we stated by simulating the Ozbudak et al. experiments. For this, we set $\mu = 0.02\ \text{min}^{-1}$ to account for the presence of a reliable carbon source (succinate) and $\phi_M = 0\ \text{min}^{-1}$ (to simulate induction with TMG which is not metabolized by β-galactosidase). Then, we calculated the bifurcation points and plotted them in the *Le* versus *Ge* parameter space, using the procedure described in Methods. We took K_A as a free parameter, and found that $K_A = 9.0 \times 10^5$ mpb gives a reasonable fit to the experimental points of Ozbudak et al. Both the model bifurcation diagram and the experimental points are presented in Fig. 3 *A*. Note that the bistability region predicted by the model is wider than the experimental one. Three possible explanations for this discrepancy are: 1), the *lac* promoter-*gfp* fusion employed by Ozbudak et al. as a reporter lacks Operators O_2 and O_3; 2), the difficulty in measuring exactly the *Le* values at which the bimodal histograms appear and disappear; and 3), the phase diagram of Fig. 3 *A* is based upon a mean-field analysis and so, biochemical noise can change the phase boundaries (25).

A fourth possible explanation for the disagreement between the model and the experimental results is that our estimated parameter values differ from those corresponding to the *E. coli* strain used by Ozbudak et al. To account for this possibility, we explored the parameter space looking for a better fit. We found that it can be obtained by decreasing the parameters ξ_i and ξ_{ij} to 20% of the values reported in Table 3, and by setting $K_A = 2.7 \times 10^6$ mpb. The results are shown in Fig. 3 *B*.

Effect of using lactose as inducer on the operon bistable behavior

The effect of using a metabolizable inducer (lactose), instead of a nonmetabolizable one (TMG), can be simulated by increasing the value of parameter ϕ_M (17). We did this for the two parameter sets described in the previous paragraph, and the results

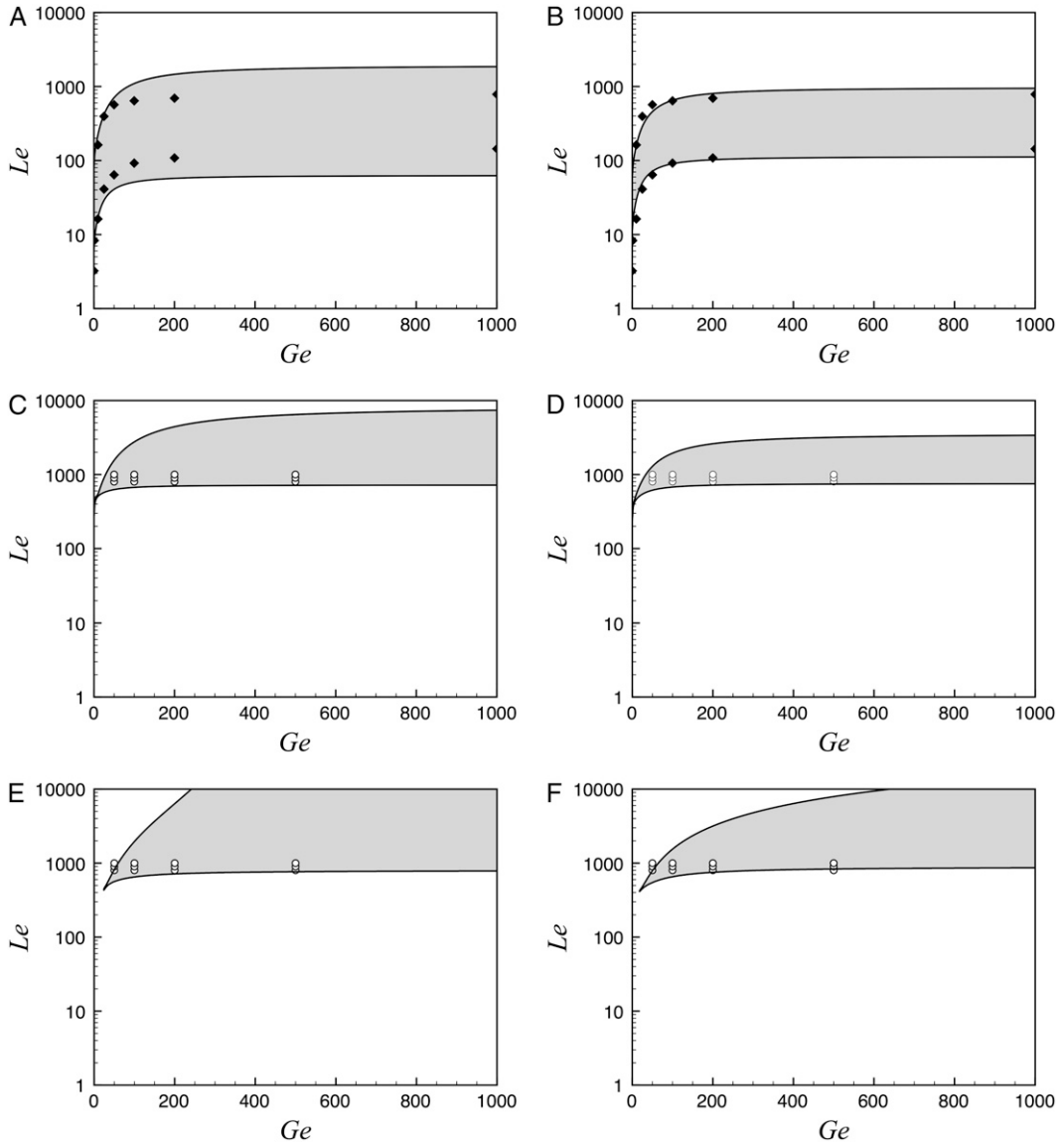

FIGURE 3 Bifurcation diagrams in the *Le* versus *Ge* parameter space, calculated with the present model under various conditions. In all cases, the bistability region is shaded, while the monostable induced (*top*) and uninduced (*bottom*) regions are uncolored. In the left column graphs we used the parameter values tabulated in Table 3, and set $K_A = 8.2 \times 10^5$ mpb. In the right column graphs all parameters ξ_i and ξ_{ij} were reduced to 0.15 times the value reported in Table 3, and K_A was set to 2.8×10^6 mpb. To calculate the graphs in the first row (*A* and *B*), we set $\phi_M = 0$ min^{-1} (to simulate induction of the *lac* operon with the nonmetabolizable TMG) and $\mu = 0.02$ min^{-1} (to simulate a bacterial culture growing in a medium that contains a reliable carbon source not affecting the *lac* operon induction). The K_A values referred to above were chosen to fit the experimental results of Ozbudak et al. (16), which are shown with solid diamonds. In the second row graphs we keep $\mu = 0.02$ min^{-1}, but increase ϕ_M to simulate the usage of lactose to induce the operon. In panel *C*, ϕ_M 3.8×10^4 min^{-1}, while in panel *D*, ϕ_M 3.0×10^4 min^{-1}. Finally, in the third row graphs, a variable growth rate was considered, together with increased ϕ_M values. The open circles in graphs *C–F* denote the *Ge* and *Le* values for which the stochastic simulations in Figs. 4–7 were carried out.

are shown in Fig. 3, *C* and *D*. Note that, although quantitatively different, the effect of lactose metabolism on the bistable behavior of the *lac* operon is qualitatively similar in both cases. Thus, bistability is not eliminated by the inclusion of lactose metabolism, but the region of bistability moves upward toward higher [*Le*] values. If the value of ϕ_M is high enough, it can render the operon induction impossible, even with extremely high [*Le*] values. Moreover, the bistable region collapses into a cusp catastrophe for extremely low [*Ge*] values. These results agree completely with those in Santillán et al. (17).

Although ϕ_M is the parameter that changes the most when TMG is substituted by lactose, other parameters like the affinity of the allolactose-repressor complex (K_A), the parameters associated to the lactose transport kinetics (k_L and κ_L), and κ_M, can change as well. We tested the sensitivity of the model bistable behavior to variations on all those pa-

rameters, and found that K_A is, by far, the most important in that respect.

There is evidence that TMG is a weaker inducer than lactose (26), and so K_A should be decreased when induction of the operon with lactose is simulated. After recalculating the bifurcation diagrams of Fig. 3, *C* and *D*, with decreased K_A values, we found that the upper boundary moves downwards along the *Le* axis quite a bit, while the lower border also moves downwards but to a lesser extent. Thus, the overall effect is that the width of the bistability region decreases when K_A is diminished. For instance, when K_A is reduced to 25%, the value used in the TMG simulations and ϕ_M is set such that the bistability-region lower border lies at $\sim Le = 1000\ \mu$M, the bistability-region width is reduced by approximately one order of magnitude.

Variable growth rate and bistability

The presence of a reliable carbon source, such as succinate, guarantees the growth of the bacterial culture at a steady rate. Although useful when designing an experiment, this is not a likely situation under natural conditions. When the growth medium contains a mixture of glucose and lactose, and no other carbon source, the bacterial growth rate is not constant but a function of the glucose uptake and the lactose metabolism rates. To investigate the influence of a variable growth rate on the bistable behavior of the *lac* operon, we recalculated the bifurcation diagrams in the *Le* versus *Ge* parameter space, using the model equations in Table 2, with the parameter sets of Fig. 3, *C* and *D*. The results are shown in Fig. 3, *E* and *F*.

Comparing Fig. 3, *C* and *E*, as well as Fig. 3, *D* and *F*, we conclude that a variable growth rate has no appreciable effect on the lower boundary of the bistable region. However, the upper border is affected. Instead of being nearly constant for moderate to high values of *Ge*, and rapidly decreasing for low *Ge* levels as in Fig. 3, *C* and *D*, the upper border increases steadily as *Ge* increases when μ is not constant. Moreover, for low to moderate *Ge* levels, the bistable region corresponding to a constant growth rate is wider than that corresponding to a variable μ, while the reverse happens for high external glucose concentrations. Another important difference is that the location of the cusp catastrophe moves to the right when a variable growth rate is considered.

We also tested the effect that decreasing the parameter K_A has on the system bistable behavior and found, again, that the width of the bistability region rapidly decreases as K_A decreases, while its lower boundary remains with little change.

Intrinsic noise and its effect on the operon dynamics

The *lacZ* mRNA degradation rate is so high that, according to the model, the average number of mRNA molecules per bacterium is $\sim$0.75 when the operon is fully induced. Therefore, there must be quite high levels if intrinsic noise, which in turn may have important effects on the system dynamic behavior. To test this, we carried out stochastic simulations (following the process outlined in the Methods section) for several conditions of external lactose and glucose. We repeated these simulations for the four parameter sets corresponding to Fig. 3, *C–F*.

In all cases, the simulations were carried out for 200,000 min to guarantee that the system reached the steady state and, if the (*Ge*, *Le*) point lies inside the bistability region, that the system state switches back and forth between the uninduced and induced states several times. Following Santillán et al. (17), we assumed that ϕ_M is $\sim 3\text{–}4 \times 10^4\ \text{min}^{-1}$. This implies that even if *Le* is as high as 1000 μM, the (*Ge*, *Le*) point lies very close to the lower border of the bistable region for moderate to high *Ge* levels.

Histograms of lactose molecule counts were calculated for each stochastic simulation. We observed that whenever the (*Ge*, *Le*) point lies below the bistability region, the histograms' maximum is very close to zero, and they quickly decay as the number of lactose molecules increase. We also carried out simulations for *Ge* and *Le* values inside the bistable region, and even a few with the (*Ge*, *Le*) point located in the induced monostable region. The histograms we obtained are presented in Figs. 4–7, which respectively correspond to the parameter sets of Fig. 3, *C–F*.

One would expect the histograms to be bimodal whenever the (*Ge*, *Le*) point is located within the bistability region; each mode corresponding to one of the two available steady states. This is clearly observed in some of the plots in Figs. 4–7, but not in as many as expected. The reason for this is that both modes are remarkably wide, and thus merge such that they are hard to distinguish separately. In general, the bimodal distributions are more prominent as the value of *Le* increases and the (*Ge*, *Le*) point moves upwards in the bistability region, and as the value of *Ge* decreases and the (*Ge*, *Le*) point approaches the cusp catastrophe.

The effect of a variable growth rate can be analyzed by comparing Figs. 4 and 6, as well as Figs. 5 and 7. Notice that the changes in the behavior of the constant and variable growth-rate histograms are consistent with the cusp catastrophe point moving right along the *Ge* axis, in the variable μ case. Interestingly, the fact that the upper border of the bistable region behaves differently in the constant and variable μ cases seems to have no effect on the histograms, except for the points that lie in the induced monostable region in the later case.

We also calculated, following the procedure detailed in the Methods section, the transition rates from the uninduced to the induced state (k_+), and from the induced to the uninduced one (k_-). We did this for each of the stochastic simulations described in the previous paragraph, and the results are shown next to the corresponding histograms in Figs. 4–7. Notice that, in all cases, k_+ increases and k_- decreases as *Le* increases; and that k_- increases and k_+ decreases as *Ge* increases. This behavior indicates that the induced (uninduced)

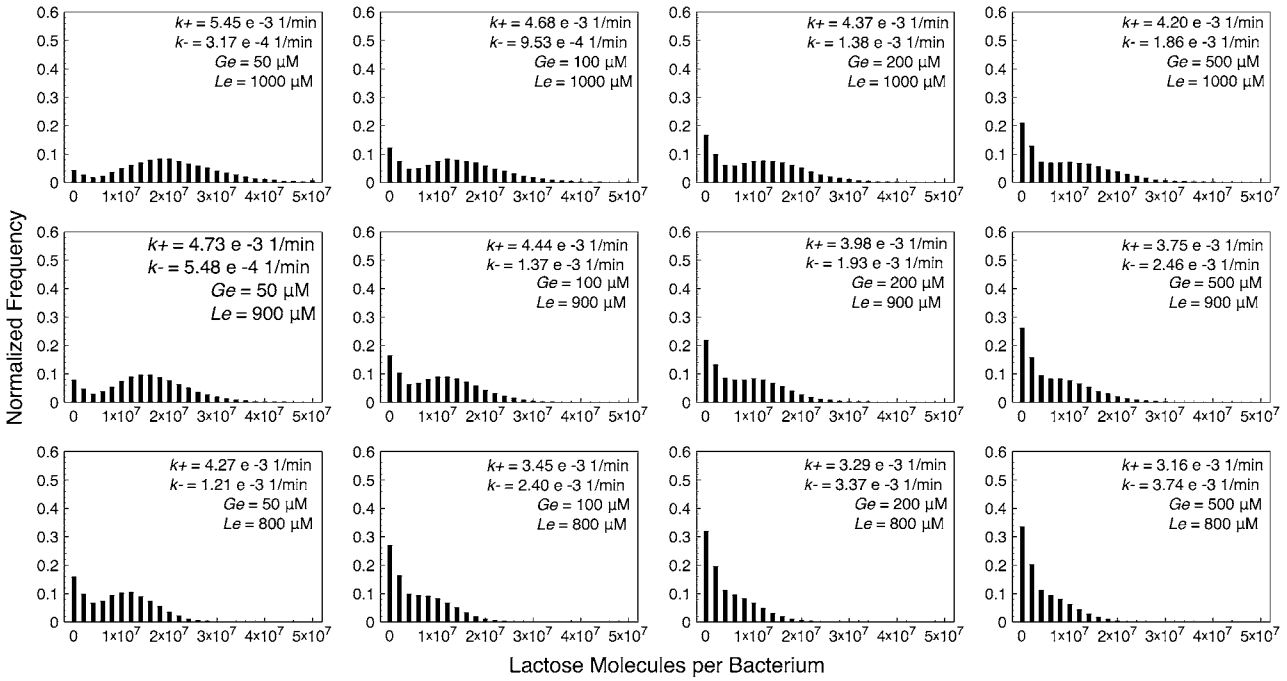

FIGURE 4 Histograms of lactose molecules per bacterium, calculated from stochastic simulations carried out with the set of parameter values corresponding to Fig. 3 *C* (constant growth rate), for different combinations of *Ge* and *Le* values. All simulations were run for 200,000 min to ensure that, if the (*Ge*, *Le*) point lies in the bistability region, the system gates several times between the uninduced and the induced states. In each histogram, the transition rates from the uninduced to the induced (k_+), and from the induced to the uninduced (k_-) states are shown.

state strengthens (weakens) its stability as the (*Ge*, *Le*) point approaches the bistability region upper boundary, and as it gets away from its lower border.

Other interesting observations that can be derived from the reported transition rates are that the residence times predicted by the model are all of $\sim 10^3$ min, and that the bimodal distributions can only be clearly noticed if $k_+ \gtrapprox 2k_-$.

Effect of the media conditions on the operon induction level and the bacterial growth rate

To better understand the dynamic performance of the *lac* operon, we numerically solved the model equations with the parameter set of Fig. 3 *E*, in which the growth rate is variable for several different levels of *Ge* and *Le*. In all cases, the numeric simulations were carried out for 2000 min to ensure that the system reaches a steady state, starting with the initial values $M = 0$ mpb, $E = 0$ mpb, and $L = 0$ mpb. Given this initial condition, the system reaches the uninduced steady state whenever it exists; otherwise, it evolves toward the induced steady state. For every one of these simulations, we recorded the β-galactosidase steady-state value, which we use as an indication of the operon induction level, and computed the corresponding steady-state growth rate. The results are shown in Fig. 8.

In Fig. 8 *A*, note that, for $Le \gtrapprox 500\,\mu$M, the system remains in the uninduced state whenever $Ge \gtrapprox 50\,\mu$M (the exact value depends on *Le*). However, there is a sudden transition to the induced state when the external glucose level decreases below a certain value. From the way we carried out the simulations, this transition corresponds to the saddle-node bifurcation in which the uninduced state disappears by colliding with the intermediate saddle node. Once the system is in the induced state, the operon induction level increases continuously until it reaches its maximum value for very low *Ge* values. However, when $200\,\mu\text{M} \lessapprox Le \lessapprox 500\,\mu$M, there is a smooth transition between the uninduced and the induced states as *Ge* decreases, in agreement with the bifurcation diagram of Fig. 3 *E*.

The operon can also be induced by increasing *Le*, given a fixed *Ge* value. We see in Fig. 8 *A* that the *lac* operon induction is smooth for $30\,\mu\text{M} \lessapprox Ge$, that the transition to the induced state is abrupt for $30\,\mu\text{M} \lessapprox Ge \lessapprox 50\,\mu$M, and that the operon never gets induced if $Le \leq 1000\ \mu$M and $50\,\mu\text{M} \lessapprox Ge$. These results are again in agreement with the bifurcation diagram of Fig. 3 *E*. In particular, the border between the smooth and abrupt transitions to the steady state corresponds to the location of the cusp catastrophe in the *Le* versus *Ge* parameter space.

Remarkably, the bacterial growth rate reaches close to maximal values for almost all combinations of *Ge* and *Le* values; see Fig. 8 *B*. The exceptions are the region just right to the border of the monostable induced region (where the value of μ is intermediate), the region of very low *Ge* and medium to high *Le* levels (where the μ-value is intermediate as well), and the region of very low *Ge* and medium to low *Le* concentrations (in which the growth rate is very close to zero).

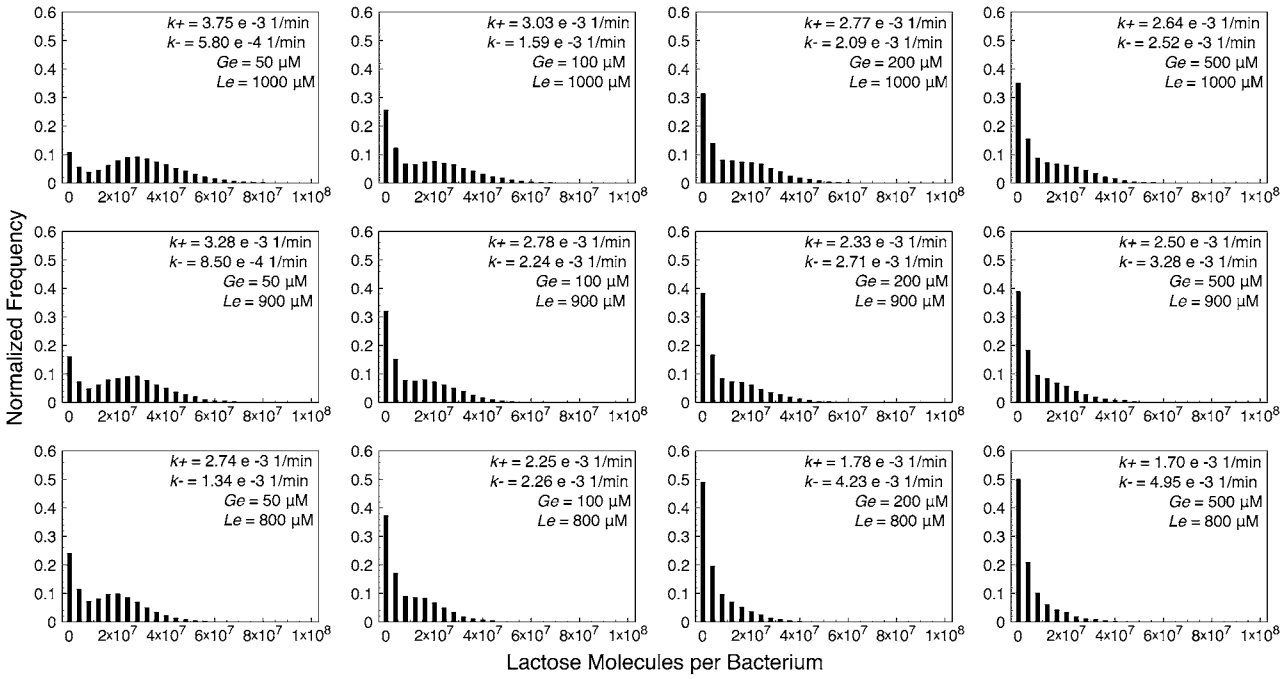

FIGURE 5 Histograms of lactose molecules per bacterium, calculated from stochastic simulations carried out with the set of parameter values corresponding to Fig. 3 *D* (constant growth rate), for different combinations of *Ge* and *Le* values. In each histogram, the transition rates from the uninduced to the induced (k_+) and from the induced to the uninduced (k_-) states are shown.

CONCLUSIONS

We have improved a previously published model for the *lac* operon in *Escherichia coli*. The improvements include: the new model takes into account the interaction between the repressor and its three different binding sites (operators) in a more detailed way; it accounts for the cooperativity between the activator (CAP) and DNA folding; and it considers the fact that the bacterial growth rate depends on the glucose uptake and the lactose metabolism rates.

Except for K_A, all the model parameters were estimated from reported experimental data. K_A was taken as a free parameter to fit the model results to the experimental data of Ozbudak et al. (16), who reported the (*Ge*, *Le*) bifurcation points corresponding to the induction of *E. coli*'s *lac* operon with TMG. We can see in Fig. 3 *A* that the bistability region predicted by the model is wider than the experimental one. In our opinion, there are four possible reasons for this discrepancy between the data and the model predictions:

- The *lac* promoter-*gfp* fusion employed by Ozbudak et al. as a reporter lacks Operators O_2 and O_3.
- Experimentally, it is quite difficult to measure with precision the *Le* values at which the bistability region starts and ends.
- The phase diagram of Fig. 3 *A* is based upon a mean-field analysis and so, biochemical noise can change the phase boundaries (25).
- The estimated parameter values differ from those corresponding to the *E. coli* strain used by Ozbudak et al.

We explored the parameter space to account for the last possibility, and found that by decreasing parameters ξ_i and ξ_{ij} to 20% of their estimated value a much better fit can be obtained (compare to Fig. 3 *B*). In all the following analysis, we used both parameter sets to test the robustness of the obtained conclusions.

Ozbudak et al. found no evidence of bistability when the natural inducer, lactose, was employed. From their simulations of the *lac* operon evolution on in silico bacterial populations, van Hoek and Hogeweg (27) proposed that the operon parameters evolve in such a way that bistability is not available for the bacteria when they grow on lactose. Santillán et al. (17) tackled this issue from a mathematical modeling viewpoint and concluded, in opposition to van Hoek and Hogeweg (27), that bistability does not disappear because of lactose metabolism, although it is very hard to identify with the Ozbudak et al. experimental setup.

Since the present model is an improvement and a generalization of the model in Santillán et al. (17), we started by corroborating their results. In Fig. 3, *C* and *D*, we can see that with a constant growth rate the current model results are in complete agreement with those of Santillán et al. (17) for the two considered parameter sets. That is, the bistability region moves upwards in the *Le* versus *Ge* parameter space, and it disappears in the region of very low *Ge* values via a cusp catastrophe. Following Santillán et al. (17), we choose the value of ϕ_M (which accounts for the maximum lactose-to-allolactose metabolism rate) such that even if $Le = 1000\ \mu M$, the (*Ge*, *Le*) point is very close to the lower border of the bistability region.

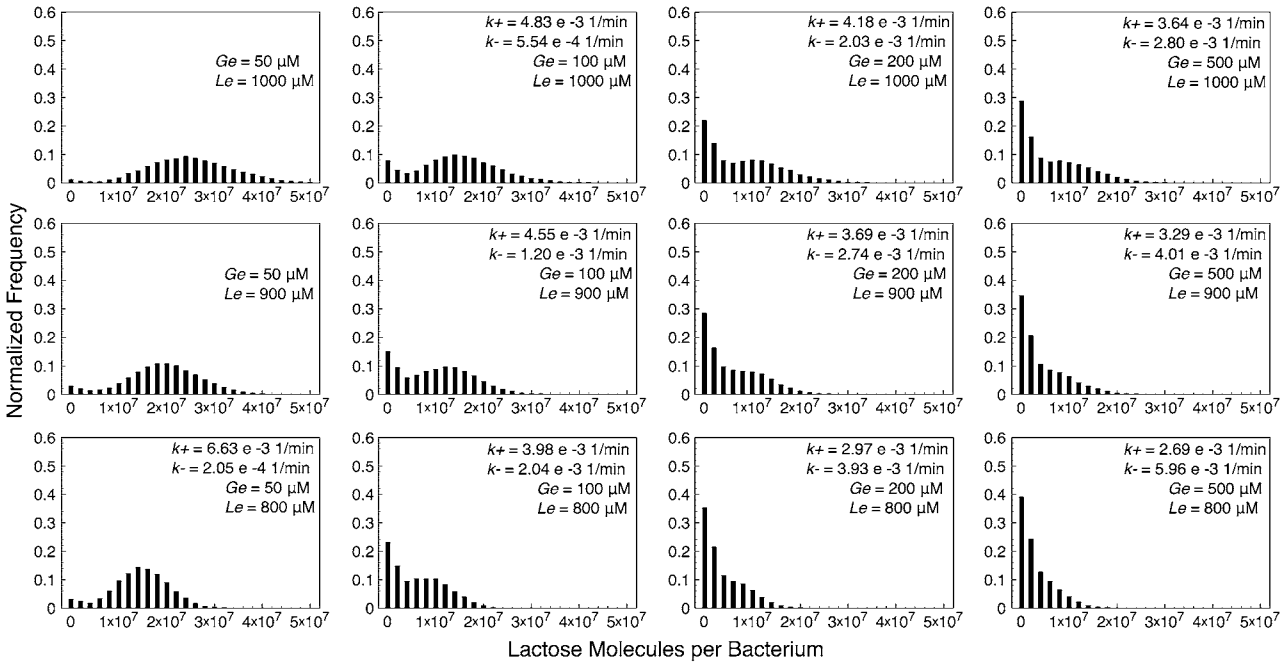

FIGURE 6 Histograms of lactose molecules per bacterium, calculated from stochastic simulations carried out with the set of parameter values corresponding to Fig. 3 *E* (constant growth rate), for different combinations of *Ge* and *Le* values. In each histogram, if bistability exists, the transition rates from the uninduced to the induced (k_+), and from the induced to the uninduced (k_-) states are shown.

Given that a constant growth rate is not realistic under natural conditions, we considered the influence of a variable μ on the bistable behavior of the *lac* operon. It can be seen in Fig. 3, *E* and *F*, that having a μ that depends on the external conditions has no appreciable effect on the lower border of the bistability region. However, the upper border is greatly modified; instead of being nearly constant from moderate to high values of *Ge* and rapidly decreasing for low *Ge* levels,

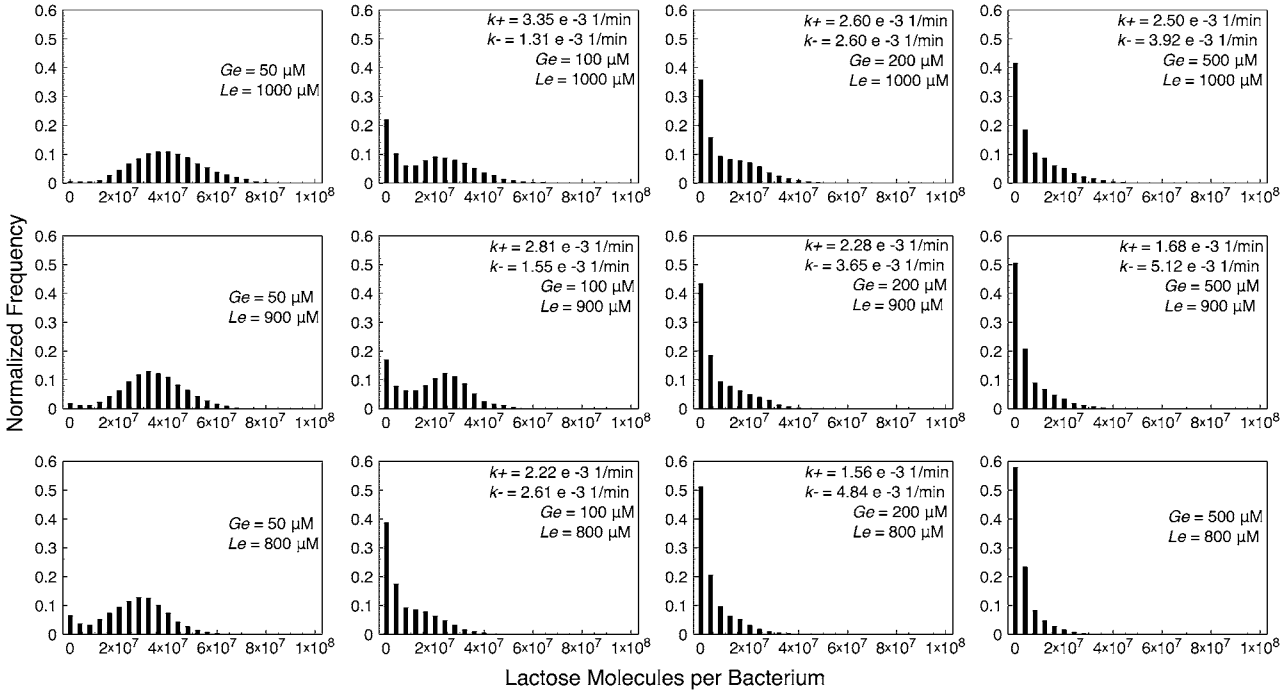

FIGURE 7 Histograms of lactose molecules per bacterium, calculated from stochastic simulations carried out with the set of parameter values corresponding to Fig. 3 *F* (constant growth rate), for different combinations of *Ge* and *Le* values. In each histogram, if bistability exists, the transition rates from the uninduced to the induced (k_+), and from the induced to the uninduced (k_-) states are shown.

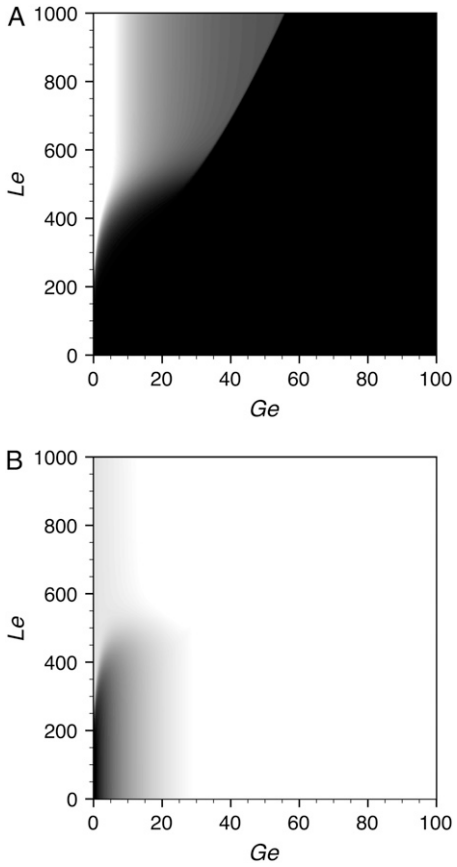

FIGURE 8 Steady-state operon induction level (A), defined as proportional to the concentration of LacZ polypeptides (E), and steady-state bacterial growth rate (B), calculated for different values of Ge and Le. For given values of Ge and Le, the E and μ steady-state values were computed by numerically solving the model equations for 2000 min, to ensure that the system reaches a steady state. This starts with the initial condition $M = 0$ mpb, $E = 0$ mpb, and $L = 0$ mpb, so the system reaches the uninduced steady state whenever it exists. Black and white, respectively, represent the minimum and maximum values of the corresponding variables in both graphs.

as in Fig. 3, C and D, the upper border increases steadily as Ge increases. Furthermore, the cusp catastrophe location moves rightwards, along the Ge axis, when a variable μ is considered.

We also carried out stochastic simulations, considering both a constant and a variable growth rate, to test how feasible the Ozbudak et al. experimental setup is to identify bistability when lactose is the inducer. According to Ozbudak et al., whenever a bimodal distribution is found, it can be considered a proof for bistability. More precisely, having a bimodal distribution is a sufficient but not a necessary condition for this behavior: for instance, if we have large standard deviations, a bimodal distribution will hardly be noticed even is bistability is present. Our numeric experiments confirm that, for the employed ϕ_M values, identifying bistability via expression-level distributions is very difficult, regardless of whether a constant or a variable growth rate is considered; compare to Figs. 4–7. It is known that the shot noise resulting from the production of multiple protein copies per mRNA transcript also lowers the switch stability (24) and probably widens the distribution, thus further blurring the bimodal distribution. This could perhaps explain why, in the experiments by Ozbudak et al., only a unimodal distribution was observed in the presence of lactose.

van Hoek and Hogeweg (27) simulated, in silico, the evolution of the *lac* operon in bacterial populations. According to their results, the parameters that determine the expression of the *lac* operon genes evolve in such a way that, when the bacterial population is grown in a medium rich in lactose, bistability disappears. Contrarily, when the bacteria grow in the presence of a gratuitous inducer, van Hoek and Hogeweg predict that bistability would be present. They propose that this behavior explains why Ozbudak et al. (16) did not observe bistability when *E. coli* was grown on lactose. From the results discussed above, we propose a different explanation; namely, that bistability does not disappear when lactose is the employed inducer, but the bistability region in the Le versus Ge parameter space is modified in such a way that this behavior is masked due to the intrinsic noise.

E. coli and other bacteria can feed on both lactose and glucose. However, when they grow in a medium rich in both sugars, glucose is utilized before lactose starts being consumed. This phenomenon, known as diauxic growth (28,29), represents an optimal thermodynamic solution given that glucose is a cheaper energy source than lactose: to take advantage of lactose, the bacteria needs to expend energy in producing the enzymes needed to transport and metabolize this sugar (30).

To test whether the results discussed above are compatible with diauxic growth and, more generally, to better understand the *lac* operon performance under variable conditions of external lactose and glucose, we calculated the plots in Fig. 8. To do that, the model equations were numerically solved for several values of Ge and Le, with the parameter set of Fig. 3 E, and with the initial condition $M = 0$ mpb, $E = 0$ mpb, and $L = 0$ mpb. This initial condition was chosen so the system reaches the uninduced steady state, unless it does not exist. In this last case, the system evolves toward the induced state.

Consider a bacterial culture growing in a medium containing a mixture of glucose and lactose. We can see from the results in Fig. 8 A (where the operon induction level is plotted versus Ge and Le) that diauxic growth is predicted by the model. That is, induction of the *lac* operon only occurs when glucose is exhausted. However, it can take place in two different ways: if $Le < 500$ μM, the cells undergo a smooth transition from the uninduced to the induced state; otherwise, the *lac* operon shifts abruptly from the off- to the on-state when glucose is almost completely depleted. Why this difference? To answer this question, we carried out numeric experiments in which the lactose operon is induced by changing the bacterial culture from a medium rich in glucose (in which it has been growing for a long time) to a medium with no glucose, while Le is kept constant. Our results (not shown) indicate that it

takes >1000 min for the *lac* operon to become fully induced when $Le = 300\ \mu$M; while, when $Le = 1000\ \mu$M, the operon achieves a 97% induction level 300 min after the medium shift. We conclude from these last results that, with a very high external lactose concentration, the *lac* operon can remain fully uninduced until glucose utilization is almost complete because the response time is short in these conditions.

In principle, it should be possible to induce the *lac* operon by increasing the *Le* value. However, the results in Fig. 8 *A* predict that, if $Ge > 60\ \mu$M, this is practically impossible for any physiological concentration of external lactose. This can be interpreted as an optimal behavior; if we consider that glucose is a cheaper carbon source, it makes sense to keep the genes in the lactose operon uninduced, as long the energy necessary to grow can be obtained from that sugar. We can also observe from Fig. 8 *A* that, when $30\ \mu\text{M} < Ge < 60\ \mu$M, the operon undergoes an abrupt transition to the induced state with high enough levels of *Le*. However, the induction level only reaches an intermediate value. Finally, if $Ge < 30\ \mu$M, the operon induction level increases smoothly as *Le* increases. In this last case, the induction level can get very close to its maximum possible value; a higher value is obtained sooner as *Ge* decreases. This behavior can also be interpreted as optimal; if the amount of glucose in the growing medium is not enough to support the bacterial population, it is reasonable to allow a continuous increase of the *lac*-operon induction level as the amount of lactose in the environment increases.

In Fig. 8 *B*, the bacterial growth rate (calculated under the same conditions as Fig. 8 *A*) was plotted versus *Ge* and *Le*. Remarkably, the value of μ is very close to its maximum almost everywhere; the only exception is the region corresponding to very low levels of *Ge* and *Le*. We conclude from this that bistability not only helps to guarantee an efficient switching of the *lac* operon in *E. coli*, when feeding on glucose, lactose, or both sugars, but also plays an important role in maintaining a high bacterial growth rate for an extremely wide range of environmental conditions.

The above discussion regarding the influence of lactose metabolism on the bistable behavior of the *lac* operon relies on the assumption that only the value of parameter ϕ_M is affected when the operon is induced with lactose instead of TMG. We know, being that TMG is a weaker inducer, K_A should be decreased as well. We investigated the sensitivity of the system bistable behavior to modifications on this parameter and found that the width of the bistability region—in the *Le* versus *Ge* parameter-space bifurcation diagram—rapidly decreases as K_A diminishes, while its lower boundary remains with little change.

These facts oblige us to reconsider our conclusions. Thus, if the change on K_A is small and the bistability region is still quite wide, then all the above stated conclusions hold like that. Otherwise, our results regarding the system behavior when the (*Ge*, *Le*) point lies within the bistability region are probably no longer valid. However, not everything is lost because, even then, bistability does not disappear, and the incapability of Ozbudak et al. to observe it can still be explained if the bistability region is so high along the *Le* axis (due to a very high ϕ_M value), that the *lac* operon never gets induced, except for extremely low *Ge* values (below the cusp catastrophe).

APPENDIX A: MODEL DEVELOPMENT

Interaction of the *lac* repressor with the operators

The *lac* repressor is a tetramer, formed by the union of two functional homodimers. Each monomer in a repressor can be bound by an allolactose molecule. When all four monomers are free, each dimer can bind any of the *lac*-operon operators. When one or the two monomers in a dimer are bound by allolactose molecules, it is unable to bind an operator; but the dimer in the opposite side still can do it, provided both their monomers are free. Finally, if either of the two monomers is on an opposite side, or three or all four monomers are bound to allolactose, none of the repressor dimers is capable of binding an operator.

Given that there are six possible configurations in which two repressor monomers are bound by allolactose molecules, and that in two of such configurations both bound monomers belong to the same dimer, we can assume that one-third of the repressors with two occupied monomers are capable of binding an operator. This assumption is supported by the fact that the binding of allolactose to a given monomer is independent of its binding to the other three monomers.

Let R, R_A, and R_{2A}, respectively, represent a free repressor, and a repressor bound by one and two allolactose molecules. They can bind an operator, O, according to the following reactions:

$$\begin{aligned} R + O &\underset{K_R/2}{\rightleftharpoons} O_R, \\ R_A + O &\underset{K_R}{\rightleftharpoons} O_{R_A}, \\ R_{2A} + O &\underset{K_R}{\rightleftharpoons} O_{R_{2A}}. \end{aligned}$$

The dissociation constant of the first reaction ($K_R/2$) is half as large as those of the second and third reactions (K_R) because, in a free repressor, both dimers can bind the operator, and therefore the forward reaction rate is twice as large.

Recalling that only one-third of the R_{2A} compounds can bind an operator, the equilibrium equations corresponding to the reactions in the former paragraph are

$$\begin{aligned} [R][O] &= \frac{K_R}{2}[O_R], \\ [R_A][O] &= K_R[O_{R_A}], \\ \frac{1}{3}[R_{2A}][O] &= K_R[O_{R_{2A}}]. \end{aligned}$$

Assume that the total concentration of operators ($[O_T]$) remains constant:

$$[O] + [O_R] + [O_{R_A}] + [O_{R_{2A}}] = [O_T].$$

Then, it follows after a little algebra that the concentration of free operators is given by

$$[O] = \frac{1}{1 + \dfrac{2[R]}{K_R} + \dfrac{[R_A]}{K_R} + \dfrac{[R_{2A}]}{3K_R}}[O_T]. \tag{20}$$

The binding of allolactose (A) to the *lac* repressor (R) takes place in four consecutive independent steps as

$$R + A \underset{K_A/4}{\rightleftharpoons} R_A, \quad R_A + A \underset{2K_A/3}{\rightleftharpoons} R_{2A},$$
$$R_{2A} + A \underset{3K_A/2}{\rightleftharpoons} R_{3A}, \quad R_{3A} + A \underset{4K_A}{\rightleftharpoons} R_{4A}.$$

The different factors multiplying the dissociation constants account for the fact that the forward and backward reaction rates are proportional to the number of empty and occupied allolactose binding sites, respectively.

The equilibrium equations for the repressor-allolactose binding reactions are

$$[R][A] = \frac{1}{4}K_A R_A, \quad [R_A][A] = \frac{2}{3}K_A[R_{2A}],$$
$$[R_{2A}][A] = \frac{3}{2}K_A[R_{3A}], \quad [R_{3A}][A] = 4K_A[R_{4A}].$$

From these and the equation accounting for the conservation of repressor molecules,

$$[R] + [R_A] + [R_{2A}] + [R_{3A}] + [R_{4A}] = [R_T],$$

it follows that $[R]$, $[R_A]$, and $[R_{2A}]$ are, respectively, given by

$$[R] = \frac{1}{(1 + [A]/K_A)^4}[R_T], \tag{21}$$

$$[R_A] = \frac{4[A]/K_A}{(1 + [A]/K_A)^4}[R_T], \tag{22}$$

$$[R_{2A}] = \frac{6([A]/K_A)^2}{(1 + [A]/K_A)^4}[R_T]. \tag{23}$$

Finally, by substituting Eqs. 21–23 into Eq. 20, we obtain the following expression for the concentration of free operators, in terms of the allolactose concentration,

$$[O] = \frac{1}{1 + \dfrac{2[\mathrm{R}']}{\mathrm{K_R}}}, \tag{24}$$

with

$$[R'] = \frac{1}{(1 + [A]/K_A)^2}[R_T]. \tag{25}$$

DNA folding

Assume that there are two different operators (or *lac* repressor binding sites) that only allolactose-free repressor molecules can bind, and that DNA can fold in such a way that a single repressor can bind both operators simultaneously. Let O, O_R^1, O_R^2, O_{2R}, and $O_R^{(12)}$, respectively, denote the binding states in which both operators are free; the first operator is bound by a repressor and the second is free; only the second operator is bound by a repressor; each operator is bound by a different repressor molecule; and both operators are bound by the same repressor through DNA folding. The chemical reactions standing for all of the transitions between these states are

$$O + R \underset{K_R^1/2}{\rightleftharpoons} O_R^1, \quad O + R \underset{K_R^2/2}{\rightleftharpoons} O_R^2,$$
$$O_R^1 + R \underset{K_R^2/2}{\rightleftharpoons} O_{2R}, \quad O_R^2 + R \underset{K_R^1/2}{\rightleftharpoons} O_{2R},$$
$$O_R^1 \underset{K_2}{\rightleftharpoons} O_R^{(12)}, \quad O_R^2 \underset{K_1}{\rightleftharpoons} O_R^{(12)}.$$

The equilibrium equations for these equations are

$$[O][R] = \frac{K_R^1}{2}[O_R^1], \quad [O][R] = \frac{K_R^2}{2}[O_R^2],$$
$$[O_R^1][R] = \frac{K_R^2}{2}[O_{2R}], \quad [O_R^2][R] = \frac{K_R^1}{2}[O_{2R}],$$
$$[O_R^1] = K_2[O_R^{(12)}], \quad [O_R^2] = K_1[O_R^{(12)}].$$

The condition that the total concentration of DNA regulatory regions remains constant is

$$[O] + [O_R^1] + [O_R^2] + [O_{2R}] + [O_R^{(12)}] = [O_T].$$

It follows from the last two equations that the probability for both operators to be free is

$$\frac{[O]}{[O_T]} = \frac{1}{1 + \dfrac{2[\mathrm{R}]}{\mathrm{K_R^1}} + \dfrac{2[\mathrm{R}]}{\mathrm{K_R^2}} + \dfrac{2[\mathrm{R}]}{\mathrm{K_R^1}}\dfrac{2[\mathrm{R}]}{\mathrm{K_R^2}} + \dfrac{[\mathrm{R}]}{\mathrm{K_R^{12}}}}, \tag{26}$$

where $K_R^{12} = K_R^1 K_2/2 = K_R^2 K_1/2$. Similarly, the probability that the first operator is free, regardless of the second operator state, is given by

$$\frac{[O] + [O_R^2]}{[O_T]} = \frac{1 + \dfrac{2[\mathrm{R}]}{\mathrm{K_R^2}}}{1 + \dfrac{2[\mathrm{R}]}{\mathrm{K_R^1}} + \dfrac{2[\mathrm{R}]}{\mathrm{K_R^2}} + \dfrac{2[\mathrm{R}]}{\mathrm{K_R^1}}\dfrac{2[\mathrm{R}]}{\mathrm{K_R^2}} + \dfrac{[\mathrm{R}]}{\mathrm{K_R^{12}}}}. \tag{27}$$

To take into account the dependence of these probabilities on the allolactose concentration, we only need to substitute R from Eq. 21.

A more realistic model should take into account the fact that all of the repressors bound by one allolactose, and one-third of those bound by two allolactose molecules, can also bind an operator, although they are unable to simultaneously bind the two operators through DNA folding. To carry out the corresponding analysis, more chemical reactions and their corresponding equilibrium equations must be included, as in the previous subsection. Although not too complicated, the whole process is quite lengthy. Therefore, we omit the details for the sake of brevity and simply give the results. For instance, the probability that both operators are free is given by

$$\frac{[O]}{[O_T]} = \frac{1}{1 + \dfrac{2[\mathrm{R}']}{\mathrm{K_R^1}} + \dfrac{2[\mathrm{R}']}{\mathrm{K_R^2}} + \dfrac{2[\mathrm{R}']}{\mathrm{K_R^1}}\dfrac{2[\mathrm{R}']}{\mathrm{K_R^2}} + \dfrac{[\mathrm{R}]}{\mathrm{K_R^{12}}}}, \tag{28}$$

where $[R]$ and $[R']$ are, respectively, given by Eqs. 21 and 25. Similarly, the probability the first operator is free, regardless of the second operator state, is

$$\frac{[O] + [O_R^2]}{[O_T]} = \frac{1 + \dfrac{2[\mathrm{R}']}{\mathrm{K_R^2}}}{1 + \dfrac{2[\mathrm{R}']}{\mathrm{K_R^1}} + \dfrac{2[\mathrm{R}']}{\mathrm{K_R^2}} + \dfrac{2[\mathrm{R}']}{\mathrm{K_R^1}}\dfrac{2[\mathrm{R}']}{\mathrm{K_R^2}} + \dfrac{[\mathrm{R}]}{\mathrm{K_R^{12}}}}. \tag{29}$$

It is not hard to see how these results are a direct generalization of the ones presented in Eqs. 24, 26, and 27.

The three operators of the *lac* operon

The lactose operon has three different operators, termed O_1, O_2, and O_3. Free *lac* repressor molecules, as well as those bound by one allolactose, and one-third of those bound by two allolactose molecules, can bind each of these operators with different dissociation constants. Moreover, free repressor molecules can bind any two of such operators simultaneously. Denote the binding state in which all

three operators are free by O; the state in which only the i^{th} operator is bound by a repressor by O_{R}^{i}; that in which operators i and j are bound by one repressor each as $O_{2\text{R}}^{\text{ij}}$; the state in which all three operators are bound by different repressor molecules as $O_{3\text{R}}$; the state in which operators i and j are bound by a single repressor as $O_{\text{R}}^{(\text{ij})}$; and that in which operators i and j are bound by a single repressor and operator k is bound by a second repressor as $O_{2\text{R}}^{(\text{ij})\text{j}}$.

By following a similar but lengthier process to that outlined in the previous subsections, one can calculate the probabilities associated to all the binding states of this system. Given the very large number of equations involved, and of their concomitant equilibrium equations, we omit the details and give the results directly.

The probability that all three operators are free is

$$\frac{[O]}{[O_{\text{T}}]}=\frac{1}{\prod\limits_{\text{i}=1,2,3}\left(1+\frac{2[\text{R}]'}{\text{K}_{\text{R}}^{\text{i}}}\right)+\sum\limits_{\substack{\sigma\in\text{P}(1,2,3)\\ \sigma_2<\sigma_3}}\left(1+\frac{2[\text{R}']}{\text{K}_{\text{R}}^{\sigma_1}}\right)\frac{[\text{R}]}{\text{K}_{\text{R}}^{\sigma_1\sigma_2}}}, \tag{30}$$

where $P(1, 2, 3)$ stands for the set of all permutations of 1, 2, 3. The probability that only the operator O_{i} is occupied by a repressor is

$$\frac{[O_{\text{R}}^{\text{i}}]}{[O_{\text{T}}]}=\frac{\frac{2[\text{R}']}{\text{K}_{\text{R}}^{\text{i}}}}{\prod\limits_{\text{i}=1,2,3}\left(1+\frac{2[\text{R}]'}{\text{K}_{\text{R}}^{\text{i}}}\right)+\sum\limits_{\substack{\sigma\in\text{P}(1,2,3)\\ \sigma_2<\sigma_3}}\left(1+\frac{2[\text{R}']}{\text{K}_{\text{R}}^{\sigma_1}}\right)\frac{[\text{R}]}{\text{K}_{\text{R}}^{\sigma_1\sigma_2}}}. \tag{31}$$

For the probability that operators O_{i} and O_{j} are bound by different repressor molecules, we have

$$\frac{[O_{2\text{R}}^{\text{ij}}]}{[O_{\text{T}}]}=\frac{\frac{2[\text{R}']}{\text{K}_{\text{R}}^{\text{i}}}\frac{2[\text{R}']}{\text{K}_{\text{R}}^{\text{j}}}}{\prod\limits_{\text{i}=1,2,3}\left(1+\frac{2[\text{R}]'}{\text{K}_{\text{R}}^{\text{i}}}\right)+\sum\limits_{\substack{\sigma\in\text{P}(1,2,3)\\ \sigma_2<\sigma_3}}\left(1+\frac{2[\text{R}']}{\text{K}_{\text{R}}^{\sigma_1}}\right)\frac{[\text{R}]}{\text{K}_{\text{R}}^{\sigma_1\sigma_2}}}. \tag{32}$$

The probability that all three operators are bound by different repressors is

$$\frac{[O_{3\text{R}}]}{[O_{\text{T}}]}=\frac{\frac{2[\text{R}']}{\text{K}_{\text{R}}^{1}}\frac{2[\text{R}']}{\text{K}_{\text{R}}^{2}}\frac{2[\text{R}']}{\text{K}_{\text{R}}^{3}}}{\prod\limits_{\text{i}=1,2,3}\left(1+\frac{2[\text{R}]'}{\text{K}_{\text{R}}^{\text{i}}}\right)+\sum\limits_{\substack{\sigma\in\text{P}(1,2,3)\\ \sigma_2<\sigma_3}}\left(1+\frac{2[\text{R}']}{\text{K}_{\text{R}}^{\sigma_1}}\right)\frac{[\text{R}]}{\text{K}_{\text{R}}^{\sigma_1\sigma_2}}}. \tag{33}$$

The probability of having operators O_{i} and O_{j} bound by a single repressor, while the other operator is free, is

$$\frac{[O_{\text{R}}^{(\text{ij})}]}{[O_{\text{T}}]}=\frac{\frac{[\text{R}]}{\text{K}_{\text{R}}^{\text{ij}}}}{\prod\limits_{\text{i}=1,2,3}\left(1+\frac{2[\text{R}]'}{\text{K}_{\text{R}}^{\text{i}}}\right)+\sum\limits_{\substack{\sigma\in\text{P}(1,2,3)\\ \sigma_2<\sigma_3}}\left(1+\frac{2[\text{R}']}{\text{K}_{\text{R}}^{\sigma_1}}\right)\frac{[\text{R}]}{\text{K}_{\text{R}}^{\sigma_1\sigma_2}}}. \tag{34}$$

Finally, the probability that operators O_{i} and O_{j} are bound by a single repressor, while the third one (O_{k}) is bound by another repressor, is

$$\frac{[O_{2\text{R}}^{(\text{ij})\text{k}}]}{[O_{\text{T}}]}=\frac{\frac{[\text{R}]}{\text{K}_{\text{R}}^{\text{ij}}}\frac{2[\text{R}']}{\text{K}_{\text{R}}^{\text{k}}}}{\prod\limits_{\text{i}=1,2,3}\left(1+\frac{2[\text{R}]'}{\text{K}_{\text{R}}^{\text{i}}}\right)+\sum\limits_{\substack{\sigma\in\text{P}(1,2,3)\\ \sigma_2<\sigma_3}}\left(1+\frac{2[\text{R}']}{\text{K}_{\text{R}}^{\sigma_1}}\right)\frac{[\text{R}]}{\text{K}_{\text{R}}^{\sigma_1\sigma_2}}}. \tag{35}$$

Once again, it is not difficult to see how these results are generalizations of those presented in Eqs. 28 and 29.

Probability of having a polymerase bound to the *lac* promoter, including catabolite repression

Let P denote a mRNA polymerase molecule. The reaction through which P binds to promoter P_1 to form the so-called close complex, P_{C}, is

$$P+P_1 \underset{\text{K}_{\text{P}}}{\rightleftharpoons} P_{\text{C}}.$$

The equilibrium equation for this reaction is

$$[P][P_1]=K_{\text{P}}[P_{\text{C}}].$$

Furthermore, the condition for conservation of promoter sites can be written as

$$[P_1]+[P_{\text{C}}]=[P_{\text{T}}].$$

Finally, it follows from the two former equations that the probability of finding a mRNA polymerase bound to promoter P_1 is

$$p_{\text{p}}=\frac{[P_{\text{C}}]}{[P_{\text{T}}]}=\frac{\frac{[\text{P}]}{\text{K}_{\text{P}}}}{1+\frac{[\text{P}]}{\text{K}_{\text{P}}}}. \tag{36}$$

In a similar fashion, the probability that a CAP molecule, C, is bound to its corresponding binding site in the DNA chain, can be calculated as

$$p_{\text{c}}=\frac{\frac{[\text{C}]}{\text{K}_{\text{C}}}}{1+\frac{[\text{C}]}{\text{K}_{\text{C}}}}.$$

In the absence of cooperativity, the probability that the mRNAP and CAP binding sites are occupied is simply the product of p_{p} and p_{c}. However, since the binding of a CAP molecule to its corresponding binding site enhances the probability that a mRNAP is bound to P_1, the probability a polymerase is bound to the promoter, regardless of the state of the CAP binding site, is

$$p_{\text{pc}}=\frac{\frac{[\text{P}]}{\text{K}_{\text{P}}}+k_{\text{pc}}\frac{[\text{P}]}{\text{K}_{\text{P}}}\frac{[\text{C}]}{\text{K}_{\text{C}}}}{1+\frac{[\text{P}]}{\text{K}_{\text{P}}}+\frac{[\text{C}]}{\text{K}_{\text{C}}}+k_{\text{pc}}\frac{[\text{P}]}{\text{K}_{\text{P}}}\frac{[\text{C}]}{\text{K}_{\text{C}}}},$$

where $k_{\text{pc}}>1$ accounts for the cooperativity between the CAP and mRNAP binding sites. After a little algebra, this last equation can be rewritten as

$$p_{\text{pc}}=\frac{p_{\text{p}}(1+p_{\text{c}}(k_{\text{pc}}-1))}{1+p_{\text{p}}p_{\text{c}}(k_{\text{pc}}-1)}. \tag{37}$$

On the other hand, the probability that a CAP molecule is bound to its corresponding site, regardless of the promoter state, is

$$p_{cp} = \frac{\frac{[C]}{K_C} + k_{pc}\frac{[P]}{K_P}\frac{[C]}{K_C}}{1 + \frac{[P]}{K_P} + \frac{[C]}{K_C} + k_{pc}\frac{[P]}{K_P}\frac{[C]}{K_C}},$$

which can be rewritten as

$$p_{cp} = \frac{p_c(1 + p_p(k_{pc} - 1))}{1 + p_p p_c(k_{pc} - 1)}. \quad (38)$$

with $\xi_i = [R_T]/K_R^i$, and $\xi_{ij} = [R_T]/K_R^{ij}$.

So far, we have not considered a newly discovered source of cooperativity in the lactose operon of *Escherichia coli* (19): a CAP molecule bound to its corresponding site not only increases the probability that a polymerase binds the promoter, but also enhances the probability that the DNA folds in such a way that a single repressor binds Operators 1 and 3 simultaneously. To take this second fact into account we assume that the loop involving Operators 1 and 3 can only form if a CAP molecule is bound to its binding site. Consequently, the equation defining $\mathcal{P}_R([A])$ is modified by multiplying the term corresponding to the state $O_R^{(13)}$ by the probability, p_{cp}, that a CAP molecule is located in its binding site. After doing this, Function $\mathcal{P}_R([A])$ transforms into

$$\mathcal{P}_R([A]) = \frac{(1 + \xi_2\rho_1([A]))(1 + \xi_3\rho_1([A])) + \xi_{23}\rho_2([A])}{\prod_{i=1,2,3}(1 + \xi_i\rho_1([A])) + \sum_{\substack{\sigma\in P(1,2,3)\\ \sigma_2<\sigma_3}}(1 + (p_{cp} - 1)\delta_{2\sigma_1})(1 + \xi_{\sigma_1}\rho_1([A]))\xi_{\sigma_2\sigma_3}\rho_2([A])},$$

Finally, p_c must be a decreasing function of $[Ge]$ since external glucose inhibits the synthesis of cAMP, which in turn implies a decrease in C, and thus in p_c (this regulatory mechanism is known as catabolite repression). Here we assume that the functional form for p_c is given by

$$p_c([Ge]) = \frac{K_G^{n_h}}{K_G^{n_h} + [Ge]^{n_h}}. \quad (39)$$

Transcription initiation and mRNA dynamics

Only when Operator O_1 is free, can a mRNA polymerase bind the promoter P_1 and start transcription. In other words, a polymerase can start transcription in the following operator binding states: O, O_R^2, O_R^3, O_{2R}^{23}, and $O_R^{(23)}$.

Let $[D]$ denote the concentration of operon copies, and k_M the maximum transcription rate of promoter P_1. From the discussion in the previous paragraph and the results of the previous subsection, the rate of transcription initiation comes out to be

$$k_M[D]p_{pc}(\mathrm{Prob}(O) + \mathrm{Prob}(O_R^2) + \mathrm{Prob}(O_R^3) + \mathrm{Prob}(O_{2R}^{23}) + \mathrm{Prob}(O_R^{(23)})),$$

where p_{pc} is given by Eq. 37. Then, from Eqs. 30–35, the rate of transcription initiation can be rewritten as

$$k_M[D]p_{pc}([Ge])\mathcal{P}_R([A]),$$

where

$$\mathcal{P}_R([A]) = \frac{(1 + \xi_2\rho_1([A]))(1 + \xi_3\rho_1([A])) + \xi_{23}\rho_2([A])}{\prod_{i=1,2,3}(1 + \xi_i\rho_1([A])) + \sum_{\substack{\sigma\in P(1,2,3)\\ \sigma_2<\sigma_3}}(1 + \xi_{\sigma_1}\rho_1([A]))\xi_{\sigma_2\sigma_3}\rho_2([A])},$$

$$\rho_1([A]) = \left(\frac{K_A}{K_A + [A]}\right)^2,$$

$$\rho_2([A]) = \left(\frac{K_A}{K_A + [A]}\right)^4,$$

where

$$\delta_{ij} = \begin{cases} 1, & i = j, \\ 0 & \text{otherwise.} \end{cases}$$

Let μ and γ, respectively, denote the bacterial growth rate and the mRNA degradation rate. From this, the differential equation governing the mRNA (M) dynamics is

$$\frac{d[M]}{dt} = k_M[D]p_{pc}([Ge])\mathcal{P}_R([A]) - (\gamma_M + \mu)[M]. \quad (40)$$

Enzyme dynamics

Let $[E]$ be the concentration of LacZ polypeptides, and k_E be the translation initiation rate of the *lacZ* mRNA. Since there are no mechanisms involved in the *lac* operon regulation at the translation level and the degradation rate for the LacZ polypeptides is negligible, as compared to the bacterial growth rate, the polypeptide dynamics are governed by

$$[\dot{E}] = k_E[M] - \mu[E]. \quad (41)$$

Let $[Q]$ and $[B]$ represent the permease and β-galactosidase concentrations, respectively. The translation initiation and degradation rates of *lacZ* and *lacY* are slightly different. Here, we assume they are the same for the sake of simplicity. From this and the fact that β-galactosidase is a homo-tetramer made up of four *lacZ* polypeptides, while permease consists of a single *lacY* polypeptide, it follows that

$$[B] = [E]/4, \quad \text{and} \quad [Q] = [E].$$

Lactose and allolactose dynamics

Let *Le* denote extracellular lactose, *L* intracellular lactose, and *A* intracellular allolactose. From the results of Ozbudak et al. (16), in the absence of external glucose the dependence of the normalized inducer uptake rate, per β-permease molecule, on the external inducer concentration is given by

$$\beta_{\mathrm{L}}([L_{\mathrm{e}}]) = \frac{[L_{\mathrm{e}}]}{\kappa_{\mathrm{L}} + [L_{\mathrm{e}}]}.$$

The results of Ozbudak et al. (16) also allow us to model the decrease in the inducer uptake rate caused by external glucose (a mechanism known as inducer exclusion) by

$$\beta_{\mathrm{G}}(Ge) = 1 - \phi_{\mathrm{G}}\frac{Ge}{\kappa_{\mathrm{G}} + Ge}.$$

Then, if k_{L} is the maximum lactose uptake rate per permease, the lactose uptake rate is

$$k_{\mathrm{L}}\beta_{\mathrm{L}}([Le])\beta_{\mathrm{G}}([Ge])[Q].$$

After being transported into the bacterium, lactose is metabolized by β-galactosidase. Approximately half of the lactose molecules are transformed into allolactose, while the rest are used directly to produce galactose. The lactose-to-allolactose metabolism rate, which as explained above equals the lactose-to-galactose metabolism rate, can be modeled as a Michaelis-Menten function (typical of catalytic reactions)

$$\phi_{\mathrm{M}}\frac{[L]}{\kappa_{\mathrm{M}} + [L]}B.$$

Therefore, the total rate of lactose metabolized per single β-galactosidase is

$$2\phi_{\mathrm{M}}\mathcal{M}([L]), \quad \text{with} \quad \mathcal{M}([L]) = \frac{[L]}{\kappa_{\mathrm{M}} + [L]}.$$

Allolactose and lactose are both metabolized into galactose by the same enzyme: β-galactosidase. Under the assumption that the allolactose production and metabolism rates are much faster than the cell growth rate, we may assume that the these two metabolic processes balance each other almost instantaneously so

$$\phi_{\mathrm{M}}\frac{[L]}{\kappa_{\mathrm{M}} + [L]}[B] \approx \phi_{\mathrm{A}}\frac{[A]}{\kappa_{\mathrm{A}} + [A]}[B].$$

On the other hand, allolactose is an isomer of lactose, and therefore we can expect that the parameters related to the metabolism kinetics of both sugars attain similar values: $\phi_{\mathrm{M}} \approx \phi_{\mathrm{A}}$ and $\kappa_{\mathrm{M}} \approx \kappa_{\mathrm{A}}$. Then

$$[A] \approx [L].$$

Finally, from all the above considerations, the differential equation that governs the intracellular lactose dynamics is

$$\frac{d[L]}{dt} = k_{\mathrm{L}}\beta_{\mathrm{L}}([Le])\beta_{\mathrm{G}}([Ge])[Q] - 2\phi_{\mathrm{M}}\mathcal{M}([L])[B] - \gamma_{\mathrm{L}}[L], \tag{42}$$

where γ_{L} is the lactose degradation rate.

Glucose transport and growth rate

Monod (31) measured the growth rate (μ) of an *E. coli* bacterial culture in a medium with glucose as the only carbon source as a function of this sugar concentration. He found the following relation:

$$\mu = a\frac{[Ge]}{[Ge] + \Phi_{\mathrm{G}}}.$$

Later Schulze and Lipe (32) demonstrated that the growth rate is proportional to the glucose input rate, J_{G}, and that J_{G} is related to the extracellular glucose concentration via a Michaelis-Menten-like function:

$$\begin{aligned} \mu &= \varepsilon J_{\mathrm{G}}([Ge]), \\ J_{\mathrm{G}}([G_{\mathrm{E}}]) &= J_{\mathrm{G}}^{\max}\frac{[Ge]}{[Ge] + \Phi_{\mathrm{G}}}. \end{aligned} \tag{43}$$

From these considerations and the fact that after being fully metabolized every lactose molecule produces two glucoselike molecules, we assume that the growth rate of a bacterial culture, growing in a medium containing a mixture of glucose and lactose, is given by

$$\mu = \varepsilon(J_{\mathrm{G}}([Ge]) + J_{\mathrm{L}}([L])), \tag{44}$$

where $J_{\mathrm{L}} = 4\phi_{\mathrm{M}}\mathcal{M}([L])[B]$ is the rate of glucoselike molecules produced via lactose metabolizing.

APPENDIX B: PARAMETER ESTIMATIONS

Since the current model is a generalization of the one introduced in Santillán et al. (17), we took most of the parameter values from the estimations in there. Nevertheless, the way repression is modeled was improved in the current model, and therefore, the corresponding parameters have to be reestimated.

Repression parameters

From the equations in Table 2, the activation of the *lac* promoter in the absence of external glucose is

$$\mathcal{X}([A]) = p'_{\mathrm{pc}}\mathcal{P}_{\mathrm{R}}^{1}([A]) + p_{\mathrm{p}}\mathcal{P}_{\mathrm{R}}^{2}([A]),$$

where

$$p'_{\mathrm{pc}} = \frac{k_{\mathrm{pc}}p_{\mathrm{p}}}{1 + p_{\mathrm{p}}(k_{\mathrm{pc}} - 1)}.$$

The repression capacity ($\mathcal{R}$) of the *lac* promoter-operator complex is defined as the ratio of promoter activity levels between the maximally induced and maximally repressed states:

$$\mathcal{R} = \frac{\lim_{[A]\to\infty}\mathcal{X}([A])}{\mathcal{X}(0)}.$$

Oehler et al. (33) measured the repression capacity of the wild-type *lac* operon (which contains all three operators), as well as that of mutant operons in which one and two operators were removed. Their results can be summarized as follows:

Present operators	Repression capacity
O_1	18
O_1 and O_2	700
O_1 and O_3	440
O_2 and O_3	2
O_1, O_2, and O_3	1300

From its definition, the value of $\mathcal{R}$ is completely determined by parameters k_{pc}, p_{p}, ξ_{i}, and ξ_{ij}. Furthermore, the removal of O_1, O_2, and O_3 can be simulated by setting $\xi_1, \xi_{12}, \xi_{13} = 0$, $\xi_2, \xi_{12}, \xi_{23} = 0$, and $\xi_3, \xi_{13}, \xi_{23} = 0$, respectively. Similarly, the removal of O_2 and O_3 can be accounted for by setting $\xi_2, \xi_3, \xi_{12}, \xi_{13}$, and $\xi_{23} = 0$. Therefore, if we take the value of k_{pc}

estimated in Santillán et al. (17), we can use the results of Oehler et al. to estimate the parameters p_p, ξ_i, and ξ_{ij}. After carrying out the whole process, we obtained

$$\begin{array}{lllllll} \xi_1 & \simeq & 17, & \xi_2 & \simeq & 0.85, & \xi_3 \simeq 0.17, \\ \xi_{12} & \simeq & 1261.7, & \xi_{13} & \simeq & 430.6, & \xi_{23} \simeq 0. \end{array}$$

Glucose transport and growth rate parameters

Schulze and Lipe (32) demonstrated that when a bacterial culture has glucose as the only carbon source, the growth rate is proportional to the glucose uptake rate. From their results, the proportionality constant can be estimated as

$$\varepsilon \simeq 5.2 \times 10^{-10} \mathrm{mbp}^{-1}.$$

Monod (31) asserts that, for *E. coli* feeding on glucose, the culture growth rate as a function of the extracellular glucose concentration obeys a Michaelis-Menten function. He also proved that the maximal growth rate is $\sim 0.23\ \mathrm{min}^{-1}$, and that the glucose concentration for which the growth rate is half-maximal is $\sim 22\ \mu$M. From this and the result in the previous paragraph, we have that

$$J_G = J_G^{\max} \frac{[Ge]}{[Ge] + \Phi_M}$$

with

$$J_G^{\max} \simeq 4.4 \times 10^7\ \mathrm{mpb\,min}^{-1}$$

and

$$\Phi_M \simeq 22\,\mu\mathrm{M}.$$

The author thanks Michael C. Mackey for helpful advice, as well as the anonymous referees whose comments and criticisms greatly helped to improve the article.

This research was partially supported by Consejo Nacional de Ciencia y Tecnología (CONACyT, Mexico), and partially carried out while the author was visiting McGill University in December, 2006.

REFERENCES

1. Jacob, F., D. Perrin, C. Sanchez, and J. Monod. 1960. Operon: a group of genes with the expression coordinated by an operator. *C. R. Hebd. Seances Acad. Sci.* 250:1727–1729.
2. Griffith, J. S. 1968. Mathematics of cellular control processes. II. Positive feedback to one gene. *J. Theor. Biol.* 20:209–216.
3. Rietkerk, M., S. F. Dekker, P. C. de Ruiter, and J. van de Koppel. 2004. Self-organized patchiness and catastrophic shifts in ecosystems. *Science.* 305:1926–1929.
4. Ferrell, J. E., Jr., and E. M. Machleder. 1998. The biochemical basis of an all-or-none cell fate switch in *Xenopus* oocytes. *Science.* 280:895–898.
5. Bagowski, C. P., and J. E. Ferrell. 2001. Bistability in the JNK cascade. *Curr. Biol.* 11:1176–1182.
6. Bhalla, U. S., P. T. Ram, and R. Iyengar. 2002. MAP kinase phosphatase as a locus of flexibility in a mitogen-activated protein kinase signaling network. *Science.* 297:1018–1023.
7. Cross, F. R., V. Archambault, M. Miller, and M. Klovstad. 2002. Testing a mathematical model of the yeast cell cycle. *Mol. Biol. Cell.* 13:52–70.
8. Pomerening, J. R., E. D. Sontag, and J. E. Ferrell, Jr. 2003. Building a cell cycle oscillator: hysteresis and bistability in the activation of Cdc2. *Nat. Cell Biol.* 5:346–351.
9. Bagowski, C., J. Besser, C. R. Frey, and J. E. J. J. Ferrell, Jr. 2003. The JNK cascade as a biochemical switch in mammalian cells: ultrasensitive and all-or-none responses. *Curr. Biol.* 13:315–320.
10. Sha, W., J. Moore, K. Chen, A. D. Lassaletta, C. S. Yi, J. J. Tyson, and J. C. Sible. 2003. Hysteresis drives cell-cycle transitions in *Xenopus laevis* egg extracts. *Proc. Natl. Acad. Sci. USA.* 100:975–980.
11. Dubnau, D., and R. Losick. 2006. Bistability in bacteria. *Mol. Microbiol.* 61:564–572.
12. Novick, A., and M. Weiner. 1957. Enzyme induction as an all-or-none phenomenon. *Proc. Natl. Acad. Sci. USA.* 43:553–566.
13. Cohn, M., and K. Horibata. 1959. Analysis of the differentiation and of the heterogeneity within a population of *Escherichia coli* undergoing induced β-galactosidase synthesis. *J. Bacteriol.* 78:613–623.
14. Maloney, L., and B. Rotman. 1973. Distribution of suboptimally induced -D-galactosidase in *Escherichia coli*. The enzyme content of individual cells. *J. Mol. Biol.* 73:77–91.
15. Chung, J. D., and G. Stephanopoulos. 1996. On physiological multiplicity and population heterogeneity of biological systems. *Chem. Eng. Sci.* 51:1509–1521.
16. Ozbudak, E. M., M. Thattai, H. N. Lim, B. I. Shraiman, and A. van Oudenaarden. 2004. Multistability in the lactose utilization network of *Escherichia coli*. *Nature.* 427:737–740.
17. Santillán, M., M. C. Mackey, and E. S. Zeron. 2007. Origin of bistability in the *lac* operon. *Biophys. J.* 92:3830–3842.
18. Narang, A. 2007. Effect of DNA looping on the induction kinetics of the *lac* operon. *J. Theor. Biol.* 247:695–712.
19. Kuhlman, T., Z. Zhang, M. H. Saier, and T. Hwa. 2007. Combinatorial transcriptional control of the lactose operon of *Escherichia coli*. *Proc. Natl. Acad. Sci. USA.* 104:6043–6048.
20. Strogatz, S. H. 1994. Nonlinear Dynamics and Chaos. Addison-Wesley, Reading, MA.
21. Gillespie, D. T. 2001. Approximate accelerated stochastic simulation of chemically reacting systems. *J. Chem. Phys.* 115:1716–1733.
22. Gillespie, D. T., and L. R. Petzold. 2003. Improved leap-size selection for accelerated stochastic simulation. *J. Chem. Phys.* 119:8229–8234.
23. Warren, P., and P. R. ten Wolde. 2004. Enhancement of the stability of genetic switches by overlapping upstream regulatory domains. *Phys. Rev. Lett.* 92:128101.
24. Warren, P., and P. R. ten Wolde. 2005. Chemical models of genetic toggle switches. *J. Phys. Chem. B.* 109:6812–6823.
25. Kepler, T. B., and T. C. Elston. 2001. Stochasticity in transcriptional regulation: origins, consequences, and mathematical representations. *Biophys. J.* 81:3116–3136.
26. Gilbert, W., and B. Müller-Hill. 1966. Isolation of the *lac* repressor. *Biophys. J.* 56:1891–1898.
27. van Hoek, M. J., and P. Hogeweg. 2006. In silico evolved *lac* operons exhibit bistability for artificial inducers, but not for lactose. *Biophys. J.* 91:2833–2843.
28. Roseman, S., and N. D. Meadow. 1990. Signal transduction by the bacterial phosphotransferase system. *J. Biol. Chem.* 265:2993–2996.
29. Narang, A. 1998. The dynamical analogy between microbial growth on mixtures of substrates and population growth of competing species. *Biotechnol. Bioeng.* 59:116–121.
30. Dekel, E., and U. Alon. 2005. Optimality and evolutionary tuning of the expression level of a protein. *Nature.* 436:588–592.
31. Monod, J. 1949. The growth of bacterial cultures. *Annu. Rev. Microbiol.* 3:371–394.
32. Schulze, K. L., and R. S. Lipe. 1964. Relationship between substrate concentration, growth rate, and respiration rate of *Escherichia coli* in continuous culture. *Arch. Mikrobiol.* 48:1–20.
33. Oehler, S., E. R. Eismann, H. Krämer, and B. Müller-Hill. 1990. The three operators of *lac* operon cooperate in repression. *EMBO J.* 9:973–979.